

**Influence of surface albedo heterogeneity on passive remote sensing**

C. Fricke et al.

# Influence of surface albedo heterogeneity on passive remote sensing of cirrus properties

C. Fricke<sup>1</sup>, A. Ehrlich<sup>1</sup>, E. Jäkel<sup>1</sup>, B. Bohn<sup>2</sup>, M. Wirth<sup>3</sup>, and M. Wendisch<sup>1</sup>

<sup>1</sup>Leipzig Institute for Meteorology, University of Leipzig, Leipzig, Germany

<sup>2</sup>Institute for Energy and Climate Research, IEK-8, Forschungszentrum Jülich GmbH, Jülich, Germany

<sup>3</sup>Department of Atmospheric Physics, DLR Oberpfaffenhofen, Germany

Received: 14 December 2012 – Accepted: 29 January 2013 – Published: 11 February 2013

Correspondence to: C. Fricke (fricke@uni-leipzig.de)

Published by Copernicus Publications on behalf of the European Geosciences Union.

Title Page

Abstract

Introduction

Conclusions

References

Tables

Figures

⏪

⏩

◀

▶

Back

Close

Full Screen / Esc

Printer-friendly Version

Interactive Discussion

## Abstract

Airborne measurements of solar spectral radiance reflected by cirrus are performed with the HALO-SR instrument onboard the High Altitude and Long Range Research Aircraft (HALO) in November 2010. The data are used to quantify the influence of surface albedo heterogeneities on the retrieval of cirrus optical thickness and crystal effective radius. Based on radiative transfer calculations the cirrus properties are derived using a standard bispectral retrieval method. Frequency distributions of the surface albedos derived from MODIS satellite observations are used to create albedo dependent lookup tables of reflected radiance. For each albedo respectively lookup table, a corresponding result for the cirrus optical thickness and effective radius is retrieved. The retrieved cloud properties are analysed in a statistical manner to investigate the influence of surface albedo heterogeneities. The results for the cirrus optical thickness are compared to HSRL-lidar derived values which allows to investigate the role of ice crystal shape in addition. It is found that if assuming aggregate ice crystals the HSRL-lidar observations fit best to the retrieved optical thickness using spectral radiance. The uncertainty in cirrus optical thickness due to uncertainties in the surface albedo is below 0.1 and thus below the instrument uncertainty. Therefore, it is concluded that for the retrieval of cirrus optical thickness the surface albedo heterogeneity is negligible. For the retrieval of cirrus effective radius, the surface albedo is of importance introducing uncertainties up to 50%. However, it was shown that the influence of the bidirectional reflectance distribution function (BRDF) is below 10% and thus smaller than the uncertainty caused by the surface albedo.

## 1 Introduction

Passive remote sensing techniques, either satellite or airplane based, for retrieving cirrus optical and microphysical parameters are well established (Hong et al., 2007; Eichler et al., 2009). However, retrievals of cirrus properties (optical and microphysical)

ACPD

13, 3783–3816, 2013

## Influence of surface albedo heterogeneity on passive remote sensing

C. Fricke et al.

Title Page

Abstract

Introduction

Conclusions

References

Tables

Figures

⏪

⏩

◀

▶

Back

Close

Full Screen / Esc

Printer-friendly Version

Interactive Discussion





Based on albedo maps derived from MODIS (Moderate Resolution Imaging Spectroradiometer), the cirrus retrieval is performed in a statistical manner to determine the effect of the surface albedo heterogeneity on the retrieved cirrus properties.

## 2 Measurements and surface albedo

### 2.1 Airborne remote sensing of cirrus using HALO-SR and HSRL

Based in Oberpfaffenhofen/Germany, HALO performed six flights during the Techno mission within German airspace. The flights were performed between 27 October and 5 November 2010. Reflected solar spectral radiance above cirrus was measured aboard HALO using the spectroradiometer system HALO-SR consisting of one downward looking optical inlet (Field of view, FOV  $\approx 2.1^\circ$ ), one bifurcated optical fibre and two spectrometers (fixed gratings, photodiode array detectors) as illustrated in Fig. 1 by photographs and a schematic sketch. The system is similarly to the spectral modular radiation measurement system (SMART)-Albedometer introduced by (Wendisch et al., 2001) and (Bierwirth et al., 2010). It monitors a spectral range from 350 nm to 2000 nm with a spectral resolution of 2 to 3 nm (full width of half maximum) for the wavelength range between 350 and 1000 nm and 9 to 16 nm for the near infrared wavelength range 1000 to 2000 nm. A measurement uncertainty up to 5% has to be considered. The nadir looking optical inlet receives the radiances reflected by clouds, atmosphere and surface within its FOV which corresponds to a footprint at the surface of e.g. 1 km<sup>2</sup> for 14 km flight altitude.

In particular the measurements on 3 and 4 November are analysed here. The HSRL-lidar profiles of backscatter ratio are presented in Fig. 2 for these two days with investigated timeframes highlighted in red. The recorded data of the 4 November 2010 flight at an altitude of about 14 km reveals between 11:00 and 11:30 UTC a homogeneous cirrus between 9 and 13 km (Fig. 2a). The flight pattern, as illustrated in Fig. 3 covers an area of approximately 3600 km<sup>2</sup> where eight rectangular flights with leg lengths of

## Influence of surface albedo heterogeneity on passive remote sensing

C. Fricke et al.

Title Page

Abstract

Introduction

Conclusions

References

Tables

Figures

⏪

⏩

◀

▶

Back

Close

Full Screen / Esc

Printer-friendly Version

Interactive Discussion



## Influence of surface albedo heterogeneity on passive remote sensing

C. Fricke et al.

Title Page

Abstract

Introduction

Conclusions

References

Tables

Figures

⏪

⏩

◀

▶

Back

Close

Full Screen / Esc

Printer-friendly Version

Interactive Discussion

approximately 20 and 50 km were performed. The flight pattern and flight altitude of the second flight were identical to the flight of 4 November. However, on 4 November 2010 the cloud field was less homogeneous than on 3 November 2010. During the flight cloudy and cloudless situations were alternating with partly two separate cloud layers below the plane. In areas with cirrus a second cloud layer was situated at about 5 km altitude below the cirrus between 8.5 and 13 km.

Radiance measurements at a single wavelength (650 nm) are shown in Fig. 4 for 3 November 2010 between 12:38 and 12:45 UTC demonstrating fluctuations in the measured radiance that results either from the heterogeneity of the surface albedo or from the variation of cloud properties. The 650 nm wavelength radiance ranges between 0.02 to 0.05  $\text{W m}^{-2} \text{nm}^{-1} \text{sr}^{-1}$ . For 1646 nm the values are lower varying between 0.002 to 0.008  $\text{W m}^{-2} \text{nm}^{-1} \text{sr}^{-1}$ . As the optical inlet is fixed to the aircraft fuselage, aircraft roll and pitch movements will cause a deviation of the viewing direction from exact nadir. To exclude any possible errors due to such a sensor misalignment, roll and/or pitch angles of the airplane larger than  $3^\circ$  were excluded from the data analysis.

## 2.2 Statistics of surface albedo from MODIS

MODIS satellite data of surface albedo from 29 October 2010 are used to assemble a frequency distribution of surface albedo representative for the investigated cases. The MODIS surface albedo (Schaaf et al., 2002) is extracted for all MODIS pixel covered by the flight track of measurements (Fig. 3). Corresponding to the two retrieval wavelengths, MODIS band B1 (620 to 670 nm) and B6 (1628 to 1652 nm) were used. In this regard, the investigated measurement data are spectrally smoothed convolved with the spectral response function of the MODIS bands. Furthermore, the data are smoothed to the footprint size of the radiance measurements. The measurement footprint results by combining the FOV of the optical inlet and the flight distance covered during the sampling time (1 to 3 s). This results in an average footprint size of about  $1 \text{ km}^2$ . Figure 5a and 5b displays the albedo frequency distribution of both bands B1 and B6. The 2-dimensional (2-D) frequency distribution offers possible pairs of surface

## Influence of surface albedo heterogeneity on passive remote sensing

C. Fricke et al.

Title Page

Abstract

Introduction

Conclusions

References

Tables

Figures

⏪

⏩

◀

▶

Back

Close

Full Screen / Esc

Printer-friendly Version

Interactive Discussion



albedo for the B1 band between 0.025–0.09 and 0.08–0.23 for the B6 band with a maximum probability of about 0.07 and 0.2 and standard deviations of 0.018 and 0.04 respectively. The high variability of surface albedo is caused by the heterogeneity of the surface area sampled during the flight. In particular agricultural, urban, forest and water. Due to the fall season, especially the forest areas lead to highly variable albedo situation. Spectral differences are caused by this surface type variability also (Bowker et al., 1985).

### 3 Retrieval of cirrus properties from HALO-SR

#### 3.1 Standard retrieval

Cirrus optical and microphysical properties were retrieved using a statistical retrieval approach based on the standard method introduced by Nakajima and King (1990). This method was initially applied to warm liquid water clouds consisting of spherical droplets but can be adapted to cirrus clouds as shown by (Eichler et al., 2009). The statistics were derived with regard to the surface albedo variability. The retrieval method utilizes the reflected radiance at a non-absorbing wavelength at 650 nm and at an absorbing wavelength of 1646 nm. Using radiative transfer calculations, lookup tables of reflected radiances at the two wavelengths are created for combinations of optical and microphysical properties. In this way the cirrus optical thickness ( $\tau$ ) and the effective radius ( $r_{\text{eff}}$ ) are obtained by interpolating the simulation to the measured radiance pair. The optical thickness of cirrus is defined as:

$$\tau = \int_{z_1}^{z_2} b_{\text{ext}}(z) dz. \quad (1)$$

$\tau$  describes the volumetric extinction coefficient  $b_{\text{ext}}$  in units of  $\text{m}^{-1}$  integrated over the cirrus vertical extend ( $z_1$  representing cloud base and  $z_2$  cloud top). It determines the fraction of radiation that is attenuated (scattered, absorbed) by the cirrus. The second retrieved parameter is the effective radius of cirrus  $r_{\text{eff}}$ , defined by:

$$r_{\text{eff}} = \frac{3}{4} \frac{\text{Volume}}{\text{Cross Section}}. \quad (2)$$

For the 1-D simulations the radiative transfer calculation package libRadtran (Mayer and Kylling, 2005) was used. The calculations are based on the DISORT II solver, a mid-latitude winter atmosphere was used, the parameterisation for molecular absorption is treated with LOWTRAN (Ricchiuzzi et al., 1998). The atmospheric aerosol is derived out of HSRL-lidar measurements of the extinction coefficients during clear sky conditions using Klett's method (Klett, 1981). The ice crystal shape is considered by parameterisations including complete phase functions simulating a mixture of different ice crystal habits (Baum et al., 2007).

### 3.2 Homogeneous surface albedo sensitivity

The influence of the surface albedo on the reflected radiance above the cirrus and the corresponding result is quantified using radiative transfer simulations. Optically thick cirrus causes high extinctions. Thus, the reflected radiance mainly results from scattering near the cloud top. In this case, the underlying surface albedo is expected to have a minor impact on both the reflected radiance above cirrus and the retrieved cirrus properties. The situation for optically thin cirrus is more complex. The reduced extinction of optically thin cirrus leads to an increased portion of transmitted downward radiation passing the cloud and being reflected by the surface back upward. The received radiance above the cirrus consists of portions reflected by the cirrus and the surface. Atmospheric scattering adds to the upward radiance as well but is negligible compared to the cirrus and surface contributions especially for the wavelength considered here.

## Influence of surface albedo heterogeneity on passive remote sensing

C. Fricke et al.

Title Page

Abstract

Introduction

Conclusions

References

Tables

Figures

⏪

⏩

◀

▶

Back

Close

Full Screen / Esc

Printer-friendly Version

Interactive Discussion







## Influence of surface albedo heterogeneity on passive remote sensing

C. Fricke et al.

Title Page

Abstract

Introduction

Conclusions

References

Tables

Figures

⏪

⏩

◀

▶

Back

Close

Full Screen / Esc

Printer-friendly Version

Interactive Discussion

5 general. Additionally, the uncertainty range differs for both examples (5–25  $\mu\text{m}$  for a) and (17–30  $\mu\text{m}$  for b).  $\tau$  and  $r_{\text{eff}}$  retrieved by the standard retrieval assuming the mean surface albedo under- or overestimate both  $\tau$  and  $r_{\text{eff}}$  to the statistical retrieval due to a nonlinear impact of surface albedo on radiative transfer (Fig. 5a and Fig. 5b). The 2-D surface albedo frequency distribution leads to uncertainties quantified by standard deviations below 0.1 for  $\tau$ . For  $r_{\text{eff}}$  both examples show differences in the uncertainty less than 5  $\mu\text{m}$ .

10 A time series of  $\sigma_{\tau}$  and  $\sigma_{r_{\text{eff}}}$  along the flight path is plotted as vertical bars in Fig. 8a ( $\sigma_{\tau}$ ) and 8b ( $\sigma_{r_{\text{eff}}}$ ). Concurrent HSRL-lidar measurements of  $\tau$  from the HSRL-lidar are plotted in addition (open triangles). The investigated cloud shows mean optical thicknesses between 0.3 and 1.5 with deviations for the retrieved  $\tau$  lower than 0.1 (Fig. 8a). The deviation between HSRL-lidar optical thickness and values derived of HALO-SR measurements ranges below 0.4 which is larger than the measurement uncertainty. Mean  $r_{\text{eff}}$  varies between 11 and 25  $\mu\text{m}$  with uncertainties between  $\pm 3 \mu\text{m}$  and  $\pm 7.5 \mu\text{m}$  as shown in Fig. 8b. The horizontal structure or temporal variability of the cloud is reproduced by both instruments although the mentioned bias.

20 While the 4 November 2010 time series features a constant cirrus, Fig. 9 illustrates a more heterogeneous time series of 3 November 2010. While  $\tau$  retrieved from the HSRL-lidar is based on the extinction between 7 and 13 km only, the statistical approach is based on the measurement signal including reflected radiation of a cloud in 5 km altitude. Thus, as shown in Fig. 9a the retrieval leads to higher values for  $\tau$  compared to values derived by the HSRL-lidar. Nevertheless, the temporal course or horizontal variability are comparable. A continuous change between cloud and cloud free areas is causing the alternating increase and decrease of  $\tau$ . The statistical retrieval approach leads to values of  $\tau$  between 0.2 and 2.8 with standard deviations below 0.1.  $\bar{r}_{\text{eff}}$  varies between 9 and 40  $\mu\text{m}$  with a higher variation of standard deviation compared to the flight of 4 November.

25 The comparison of 3 and 4 November indicates that the standard deviation is proportional to the optical thickness which is shown in a correlation plot in Fig. 10. For

both time series  $\sigma_{r_{\text{eff}}}$  decreases with increasing  $\tau$  indicating a systematic relationship between both quantities. For the 4 November (Fig. 10a) the standard deviation reaches values between 40 % and 50 % for  $\tau = 0.5$  while it decreases to standard deviations of 20 % for  $\tau = 1.5$ . A similar correlation is observed for 3 November (Fig. 10b) with the coefficient of variation decreasing to 10 % for  $\tau = 2.5$  in Fig. 10b as higher values for  $\tau$  occurred here. The reason for the decreasing standard deviation is the decreasing influence of the surface albedo with increasing  $\tau$  when less radiation is transmitted through the cirrus as shown in Fig. 6. Unlike the small deviations for the retrieved  $\tau$ , the results for  $r_{\text{eff}}$  offer a high sensitivity to the values for  $\tau$  as expected.

## 5 Systematic and microphysical uncertainties

### 5.1 Shape effects

To investigate systematic differences between HSRL-lidar and HALO-SR measurements, the optical thickness derived from both are compared in a scatter plot in Fig. 11.

Generally both results do not agree within the uncertainty bars for most of the measurements. For low optical thicknesses ( $\tau \leq 0.5$ ) the results derived by the statistical retrieval are lower than the HSRL-lidar data of  $\tau$ . With increasing  $\tau$  the opposite is observed indicated by a slope of 0.38. One possible reason is the influence of the ice crystal shape. Non-spherical ice crystals in cirrus are considered in all radiative transfer simulations shown so far using an ice crystal parameterisation by (Baum et al., 2007), which represents a mixture of different crystal shapes. To investigate the influence of this shape assumptions all simulations are repeated by applying different ice crystal shape parameterisations. Four different shapes are taken into account: plates, droxtals, solid-columns and aggregates (Yang et al., 2000). The results are presented in Fig. 12.

In general there is still an overestimation of  $\tau$  for all shapes. Considering the slopes, the crystal shape is affecting the result for  $\tau \geq 0.5$  with increasing magnitude. The

Title Page

Abstract

Introduction

Conclusions

References

Tables

Figures

⏪

⏩

◀

▶

Back

Close

Full Screen / Esc

Printer-friendly Version

Interactive Discussion

result for droxtal shape shows the largest difference compared to the HSRL-lidar (slope = 0.38). Solid (slope = 0.51) and hollow-columns (slope = 0.56) lead to a smaller deviation in comparison to the assumption of droxtals. However, the aggregate parameterisation gives the best match within the available value range of  $\tau$ . This indicates that the most likely aggregate ice crystals were present in the observed cirrus during the time series of measurement although no perfect agreement is obtained with a slope of 0.71.

## 5.2 Grid density

Independent of the chosen crystal shape a general overestimation of  $\tau$  is observed. It is caused by a systematic feature of the statistical retrieval approach. In Fig. 13 three radiance grids following the approach of Nakajima and King (1990) for three different assumptions of the surface albedo at 650 nm (0.05, 0.1, 0.2) are displayed. Measurements are shown by triangles for a thin cloud and squares for a thick cloud. Changing the radiance grid from albedo = 0.15 to albedo = 0.25, the measurements for the thin cloud mostly fall out of the grid which means no value is retrieved. For the thick cloud this does not occur as the grid covers a larger value range in this region. We counted the number of grids (albedo values) for which a retrieval could be applied. The total number is plotted against the optical thickness in Fig. 13b. For decreasing  $\tau$  the number of solution grid points is decreasing as these solution grids are nonlinear. The consequence is a slight over- or underestimation depending on the surface albedo distribution. It is affecting both the retrieval of  $\tau$  and  $r_{\text{eff}}$ . Figure 14 illustrates the systematic feature in a retrieval of  $r_{\text{eff}}$  for different values of assumed surface albedo. Here an underestimation can be observed which is caused by the systematic retrieval feature only as different surface albedo assumptions lead to similar results.

# Influence of surface albedo heterogeneity on passive remote sensing

C. Fricke et al.

Title Page

Abstract

Introduction

Conclusions

References

Tables

Figures

⏪

⏩

◀

▶

Back

Close

Full Screen / Esc

Printer-friendly Version

Interactive Discussion

### 5.3 Bidirectional reflectance distribution function

Investigations up to this point considered an isotropic reflecting surface that reflects and scatters equal to all directions. To analyse possible angular dependent scattering effects the spectral MODIS BRDF product from 1 November 2010 has been implemented into the retrieval. The BRDF algorithm makes use of 16-day multi-data to derive parameters describing the bidirectional reflectance function that relies on the weighted sum of three parameters to determine the reflectance (Schaaf et al., 2002). It consists of one isotropic parameter ( $f_{\text{iso}}(\lambda)$ ) and two functions ( $f_{\text{vol}}(\lambda)$ ,  $f_{\text{geo}}(\lambda)$ ) of viewing and illumination geometry. While the statistic retrieval using isotropic surface scattering relies on one dimension for the albedo value for each wavelength, the BRDF adds two more dimensions for each wavelength that have to be considered. This leads to an exponential increase in calculation times not feasible for all the statistic retrieval. In consequence the amount of MODIS pixels was reduced by choosing one-tenth random values out of the whole value range of surface BRDF. Tables 1 and 2 show mean values and standard deviations of the original and the reduced random value BRDF weighting parameter ( $f_{\text{iso}}$ ,  $f_{\text{vol}}$ ,  $f_{\text{geo}}$ ) distribution for the B1 and B6 wavelength range proving comparable statistics regarding the value ranges presented in Sect. 3.2.

The comparison between the retrieval of  $\tau$  using isotropic reflecting surface albedo and the BRDF is presented in Fig. 15 based on a mixture of different ice crystal shapes.

Mean values of both  $\tau$  retrievals generally agree as the deviations range within  $\pm 0.2$ . The standard deviations range within 0.1 for both retrievals. However, the standard deviations are slightly larger in some cases for the BRDF case which can be explained by the differences in the total amount of surface albedo values affecting the retrieval. Nevertheless the influence of the BRDF on the retrieval of  $\tau$  is minimal in comparison to the general influence of the surface albedo.

The influence of the BRDF on the retrieval of  $r_{\text{eff}}$  is presented in Fig. 16.

As for  $\tau$  the retrieval of  $r_{\text{eff}}$  leads to comparable results as the numeric deviations between both mean value retrievals range within  $\pm 2.5 \mu\text{m}$ . The standard deviations of

## Influence of surface albedo heterogeneity on passive remote sensing

C. Fricke et al.

Title Page

Abstract

Introduction

Conclusions

References

Tables

Figures



Back

Close

Full Screen / Esc

Printer-friendly Version

Interactive Discussion



## Influence of surface albedo heterogeneity on passive remote sensing

C. Fricke et al.

Title Page

Abstract

Introduction

Conclusions

References

Tables

Figures

⏪

⏩

◀

▶

Back

Close

Full Screen / Esc

Printer-friendly Version

Interactive Discussion



the BRDF retrieval show no significant differences to the isotropic retrieval. The slightly larger standard deviations in some cases in the  $\tau$  retrieval are not reproduced for the  $r_{\text{eff}}$  retrieval of this time series. This states, that the BRDF influence is minimal for the  $r_{\text{eff}}$  as the directional scattering is most significant at lower wavelength related to the cirrus optical thickness.

## 6 Conclusions

The influence of surface albedo heterogeneities on the retrieval of cirrus microphysical and optical properties measured with HALO-SR has been investigated. Applying a statistical approach the uncertainties of  $\tau$  and  $r_{\text{eff}}$  related to the assumption of surface albedo are quantified by deriving the standard deviation in addition to the mean value. For the cirrus optical thickness the standard deviation is below 0.1. This shows that the presented statistical method is suitable for retrieving cloud optical thicknesses over heterogeneous surface situations when the surface albedo is not known. It has to be pointed out that these results apply only for the cirrus analysed here. The results depend on the surface albedo frequency distribution applied to the performed retrieval. In general, the uncertainty increases with increasing width of the surface albedo distribution.

For the effective radius retrieval the surface albedo sensitivity depends on the cirrus optical thickness. The larger the cirrus optical thickness the larger the uncertainty of the effective radius with regard to the surface albedo heterogeneity. Uncertainties caused by the ice crystal shape are observed for optical thicknesses larger than 0.5 and can be neglected for lower values. A comparison with the optical thickness from HSRL-lidar measurements showed best agreement for aggregates. This limit is also applicable to systematic issues relating to the retrieval approach itself. The influence of the bidirectional reflectance distribution function (BRDF) is minimal as it shows no significant differences to the use of isotropic reflecting surface albedo. One possible source of uncertainty needs to be investigated in the future. At this point the radia-

tive transfer calculations are performed in a 1-D approach leaving out possible 3-D atmospheric scattering effects which are not taken into account yet. This has to be investigated using 3-D radiative transfer modelling which will be addressed in further investigations.

- 5 *Acknowledgements.* We are grateful for funding of project WE 1900/21-1, WE 1900/22-1, WE 1900/24-1 and WE 1900/24-1 and BO 1580/4-1 by Deutsche Forschungsgemeinschaft within the framework of HALO SPP 1294. Furthermore we appreciate the assistance from DLR-FX during the campaign.

## References

- 10 Baum, B. A., Yang, P., Nasiri, S., Heidinger, A. K., Heymsfield, A., and Li, J.: Bulk scattering properties for the remote sensing of ice clouds. Part III: High-resolution spectral models from 100 to 3250  $\text{cm}^{-1}$ , *J. Appl. Meteor.*, 46, 423–434, 2007. 3789, 3793
- Bierwirth, E., Wendisch, M., Jakel, E., Ehrlich, A., Schmidt, K. S., Stark, H., Pilewskie, P., Esselborn, M., Gobbi, G. P., Ferrare, R., Muller, T., and Clarke, A.: A new method  
15 to retrieve the aerosol layer absorption coefficient from airborne flux density and actinic radiation measurements RID E-7433-2010, *J. Geophys. Res.-Atmos.*, 115, D14211, doi:10.1029/2009JD013636, 2010. 3786
- Bowker, D., Davis, R., Myrick, D., Stacy, K., and Jones, W.: Spectral Reflectances of Natural Targets for Use in Remote Sensing Studies, NASA RP-1139, NASA Langley Research Center, Hampton (VA), USA, 1985. 3788
- 20 Eichler, H., Ehrlich, A., Wendisch, M., Mioche, G., Gayet, J.-F., Wirth, M., Emde, C., and Minikin, A.: Influence of ice crystal shape on retrieval of cirrus optical thickness and effective radius: A case study, *J. Geophys. Res.*, 114, D19203, doi:10.1029/2009JD012215, 2009. 3784, 3788
- Esselborn, M., Wirth, M., Fix, A., Tesche, M., and Ehret, G.: Airborne high spectral resolution  
25 lidar for measuring aerosol extinction and backscatter coefficients, *Appl. Optics*, 47, 346–358, 2008. 3785
- Gao, B. C., Han, W., Tsay, S. C., and Larsen, N. F.: Cloud detection over the Arctic region using airborne imaging spectrometer data during the daytime, *J. Appl. Meteorol.*, 37, 1421–1429, doi:10.1175/1520-0450(1998)037<1421:CDOTAR>2.0.CO;2, 1998. 3785

## Influence of surface albedo heterogeneity on passive remote sensing

C. Fricke et al.

Title Page

Abstract

Introduction

Conclusions

References

Tables

Figures

⏪

⏩

◀

▶

Back

Close

Full Screen / Esc

Printer-friendly Version

Interactive Discussion



## Influence of surface albedo heterogeneity on passive remote sensing

C. Fricke et al.

Title Page

Abstract

Introduction

Conclusions

References

Tables

Figures

⏪

⏩

◀

▶

Back

Close

Full Screen / Esc

Printer-friendly Version

Interactive Discussion

- Hong, G., Yang, P., Gao, B. C., Baum, B. A., Hu, Y. X., King, M. D., and Platnick, S.: High cloud properties from three years of MODIS Terra and Aqua collection-4 data over the Tropics, *J. Appl. Meteor. Clim.*, 46, 1840–1856, 2007. 3784
- Klett, J. D.: Stable analytical inversion solution for processing lidar returns., *Appl. Opt.*, 20, 211–220, 1981. 3789
- Mayer, B. and Kylling, A.: Technical note: The libRadtran software package for radiative transfer calculations – description and examples of use, *Atmos. Chem. Phys.*, 5, 1855–1877, doi:10.5194/acp-5-1855-2005, 2005. 3789
- Nakajima, T. and King, M.: Determination of the optical thickness and effective particle radius of clouds from reflected solar radiation measurements. Part I: Theory, *J. Atmos. Sci.*, 47, 1878–1893, 1990. 3788
- Ricchiazzi, P., Yang, S., Gautier, C., and Sowle, D.: SBDART: A research and Teaching software tool for plane-parallel radiative transfer in the Earth's atmosphere, *B. Am. Meteorol. Soc.*, 79, 2101–2114, 1998. 3789
- Sassen, K., Wang, Z., and Liu, D.: Global distribution of cirrus clouds from CloudSat/Cloud-Aerosol Lidar and Infrared Pathfinder Satellite Observations (CALIPSO) measurements, *J. Geophys. Res.*, 113, D00A12, doi:10.1029/2008JD009972, 2008. 3785
- Schaaf, C. B., Gao, F., Strahler, A. H., Lucht, W., Li, X. W., Tsang, T., Strugnell, N. C., Zhang, X. Y., Jin, Y. F., Muller, J. P., Lewis, P., Barnsley, M., Hobson, P., Disney, M., Roberts, G., Dunderdale, M., Doll, C., d'Entremont, R. P., Hu, B. X., Liang, S. L., Privette, J. L., and Roy, D.: First operational BRDF, albedo nadir reflectance products from MODIS, *Remote Sens. Environ.*, 83, 135–148, 2002. 3787, 3795
- Wendisch, M., Müller, D., Schell, D., and Heintzenberg, J.: An airborne spectral albedometer with active horizontal stabilization, *J. Atmos. Ocean. Technol.*, 18, 1856–1866, 2001. 3786
- Wirth, M., Fix, A., Mahnke, P., Schwarzer, H., Schrandt, F., and G., E.: The airborne multi-wavelength water vapor differential absorption LIDAR WALES: system design and performance, *Appl. Phys. B: Lasers and Optics*, 96, 201–213, 2009. 3785
- Yang, P., Liou, K. N., Wyser, K., and Mitchell, D.: Parameterization of the scattering and absorption properties of individual ice crystals, *J. Geophys. Res.*, 105, 4699–4718, 2000. 3793

## Influence of surface albedo heterogeneity on passive remote sensing

C. Fricke et al.

**Table 1.** Statistic comparison between original and reduced random number BRDF distribution weighting parameters ( $f_{\text{iso}}$ ,  $f_{\text{vol}}$ ,  $f_{\text{geo}}$ ) for the B1 wavelength range.

Parameter	Mean Value		Standard Deviation	
	BRDF	BRDF <sub>reduced</sub>	BRDF	BRDF <sub>reduced</sub>
$f_{\text{iso}}$ (620–670 nm)	0.0659	0.0623	0.0205	0.0180
$f_{\text{vol}}$ (620–670 nm)	0.0306	0.0274	0.0134	0.0113
$f_{\text{geo}}$ (620–670 nm)	0.0105	0.0099	0.0046	0.0037

Title Page

Abstract

Introduction

Conclusions

References

Tables

Figures

◀

▶

◀

▶

Back

Close

Full Screen / Esc

Printer-friendly Version

Interactive Discussion

## Influence of surface albedo heterogeneity on passive remote sensing

C. Fricke et al.

**Table 2.** Statistic comparison between original and reduced random number BRDF distribution weighting parameters ( $f_{\text{iso}}$ ,  $f_{\text{vol}}$ ,  $f_{\text{geo}}$ ) for the B6 wavelength range.

Parameter	Mean Value		Standard Deviation	
	BRDF	BRDF <sub>reduced</sub>	BRDF	BRDF <sub>reduced</sub>
$f_{\text{iso}}$ (1628–1652 nm)	0.1857	0.1995	0.0408	0.0379
$f_{\text{vol}}$ (1628–1652 nm)	0.0999	0.0981	0.0341	0.0331
$f_{\text{geo}}$ (1628–1652 nm)	0.0207	0.0232	0.0094	0.0095

[Title Page](#)
[Abstract](#)
[Introduction](#)
[Conclusions](#)
[References](#)
[Tables](#)
[Figures](#)
[Back](#)
[Close](#)
[Full Screen / Esc](#)
[Printer-friendly Version](#)
[Interactive Discussion](#)

## Influence of surface albedo heterogeneity on passive remote sensing

C. Fricke et al.

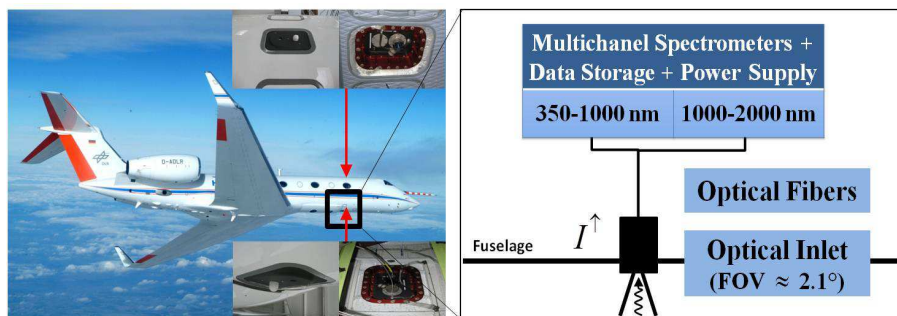


**Fig. 1.** Illustration of the HALO-SR measurement setup on HALO consisting of an optical inlet ( $\text{FOV} \approx 2.1^\circ$ ), spectrometers and a bifurcated optical fiber which transmits the signal from the optical inlet to two Zeiss multispectral spectrometers monitoring from 350 nm to 2000 nm.

Title Page

Abstract

Introduction

Conclusions

References

Tables

Figures

◀

▶

◀

▶

Back

Close

Full Screen / Esc

Printer-friendly Version

Interactive Discussion

## Influence of surface albedo heterogeneity on passive remote sensing

C. Fricke et al.

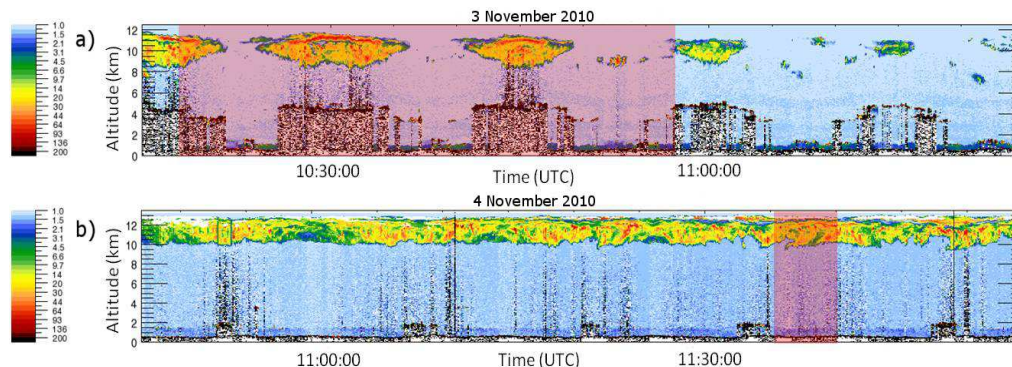


**Fig. 2.** (a) Backscatter ratio from HSRL-lidar for a 75 min timeframe of the flight of 3 November 2010 showing two descending cloud layers alternating with cloud free areas. One cloud layer is situated between 9 and 13 km altitude, a second one below 5 km altitude. The investigated time series is highlighted in red. (b) Backscatter ratio from HSRL-lidar for a 75 min timeframe of the flight of 4 November 2010 showing a constant but heterogeneous cirrus situation between 9 and 13 km altitude. The investigated time series is highlighted in red.

## Influence of surface albedo heterogeneity on passive remote sensing

C. Fricke et al.

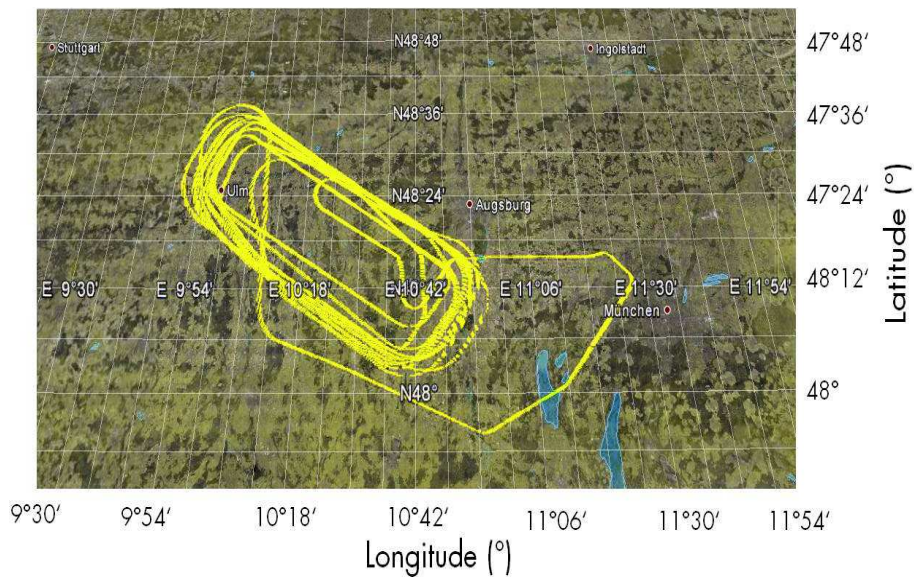


**Fig. 3.** Flight track of 3 November 2010 over the measurement area in southern Germany (illustrated using Google Earth).

Title Page

Abstract

Introduction

Conclusions

References

Tables

Figures

⏪

⏩

◀

▶

Back

Close

Full Screen / Esc

Printer-friendly Version

Interactive Discussion



## Influence of surface albedo heterogeneity on passive remote sensing

C. Fricke et al.

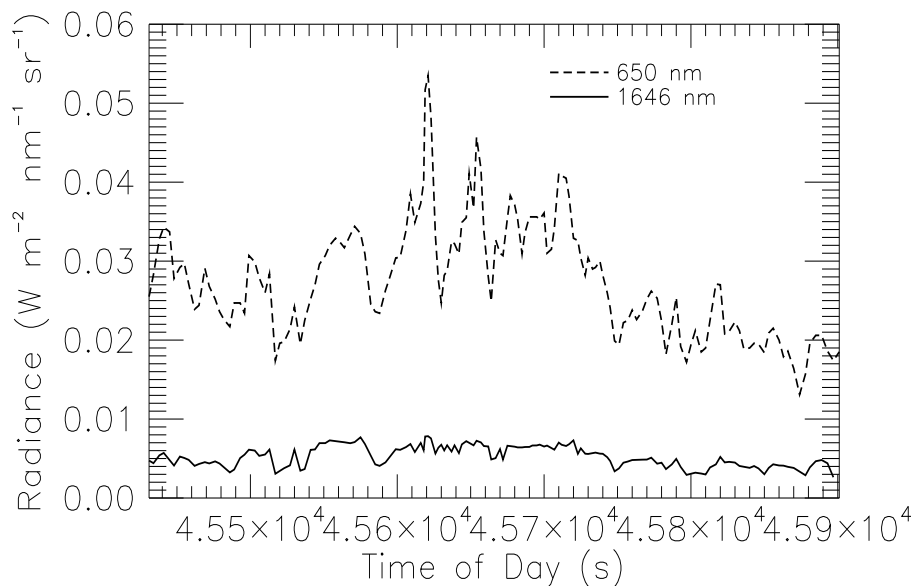


**Fig. 4.** Example timeseries of HALO-SR radiance measurement reflected by the cirrus on 3 November 2010 for two wavelengths. Variability in the measured radiance results either from the heterogeneity of surface albedo or cloud properties.

Title Page

Abstract

Introduction

Conclusions

References

Tables

Figures

⏪

⏩

◀

▶

Back

Close

Full Screen / Esc

Printer-friendly Version

Interactive Discussion

## Influence of surface albedo heterogeneity on passive remote sensing

C. Fricke et al.

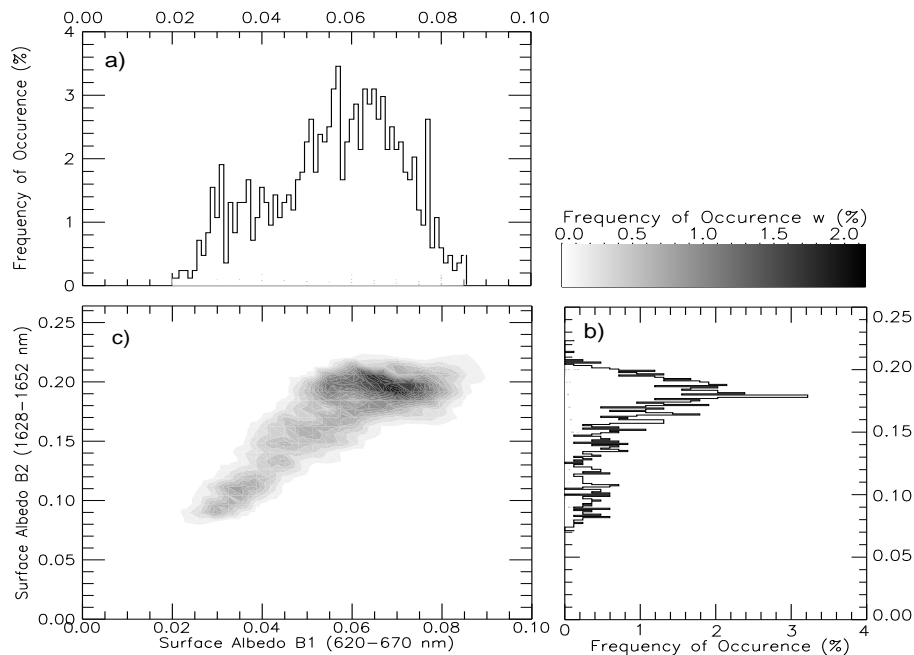


**Fig. 5.** 2-dimensional (2-D) frequency distribution of the combined B1 and B6 surface albedo for the flight track. Each value stands for a surface albedo pair with bin size of 0.005. In panel **(a)** and **(b)** the separate B1 and B6 distributions are displayed.

[Title Page](#)
[Abstract](#)
[Introduction](#)
[Conclusions](#)
[References](#)
[Tables](#)
[Figures](#)
[⏪](#)
[⏩](#)
[⏴](#)
[⏵](#)
[Back](#)
[Close](#)
[Full Screen / Esc](#)
[Printer-friendly Version](#)
[Interactive Discussion](#)

## Influence of surface albedo heterogeneity on passive remote sensing

C. Fricke et al.

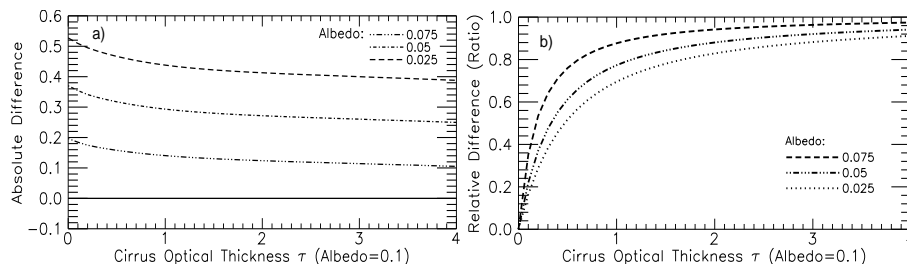


**Fig. 6.** Absolute (a) and relative difference (ratio) (b) between the result of a retrieval of  $\tau$  to the given values derived by creating a cirrus with optical thicknesses between 0 and 4 and a fixed surface albedo of 0.1 and the same retrieval assuming a surface albedo of 0.025, 0.05 and 0.075.

[Title Page](#)
[Abstract](#)
[Introduction](#)
[Conclusions](#)
[References](#)
[Tables](#)
[Figures](#)
[⏪](#)
[⏩](#)
[◀](#)
[▶](#)
[Back](#)
[Close](#)
[Full Screen / Esc](#)
[Printer-friendly Version](#)
[Interactive Discussion](#)

## Influence of surface albedo heterogeneity on passive remote sensing

C. Fricke et al.

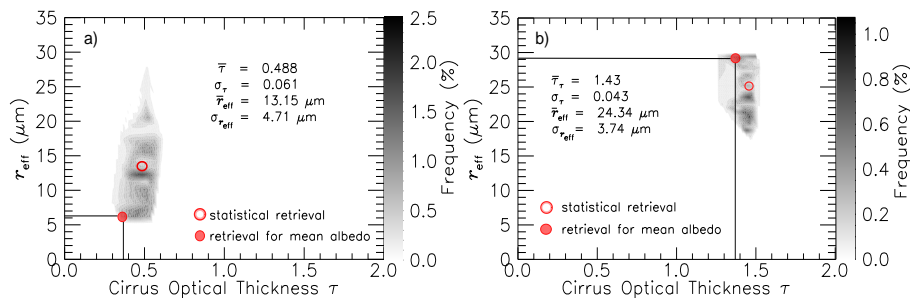


**Fig. 7.** Frequency distribution of  $\tau$  and  $r_{\text{eff}}$  of two HALO-SR measurement examples ((a) 40601 s, (b) 40795 s) for the flight of 4 November 2010. The red filled dot indicates the result for assuming the mean surface albedo compared to statistic retrieval values (blank dot).

Title Page

Abstract

Introduction

Conclusions

References

Tables

Figures

◀

▶

◀

▶

Back

Close

Full Screen / Esc

Printer-friendly Version

Interactive Discussion

## Influence of surface albedo heterogeneity on passive remote sensing

C. Fricke et al.

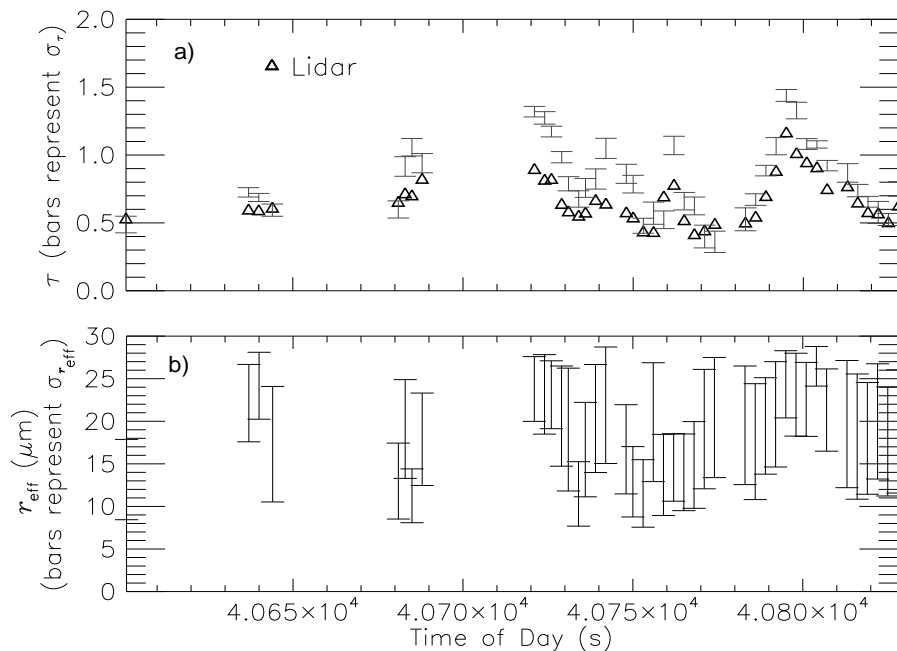


**Fig. 8.** (a) Comparison between  $\sigma_\tau$  of statistic retrieval (bars) derived of HALO-SR measurements and values derived of the HSRL-lidar (triangle) from the 4 November 2010 flight between 11:00 and 11:30 UTC. Gaps are caused by roll movements of the plane, where nadir measurements could not be obtained. (b)  $\sigma_{r_{\text{eff}}}$  of the corresponding time.

[Title Page](#)
[Abstract](#)
[Introduction](#)
[Conclusions](#)
[References](#)
[Tables](#)
[Figures](#)
[⏪](#)
[⏩](#)
[◀](#)
[▶](#)
[Back](#)
[Close](#)
[Full Screen / Esc](#)
[Printer-friendly Version](#)
[Interactive Discussion](#)

## Influence of surface albedo heterogeneity on passive remote sensing

C. Fricke et al.

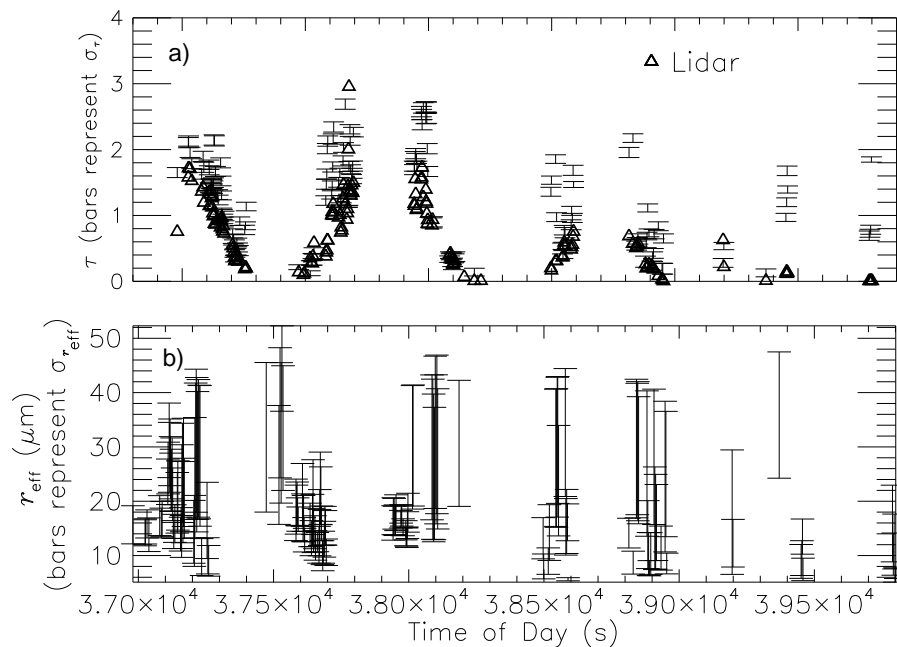


**Fig. 9.** (a) Comparison between  $\sigma_\tau$  of statistic retrieval (bars) derived of HALO-SR measurements and values derived of the HSRL-lidar (triangle) from the 3 November 2010 flight between 10:15 and 11:00 UTC. Gaps are caused by roll movements of the plane, where nadir measurements could not be obtained. (b)  $\sigma_{r_{\text{eff}}}$  of the corresponding timeframe.

[Title Page](#)
[Abstract](#)
[Introduction](#)
[Conclusions](#)
[References](#)
[Tables](#)
[Figures](#)
[Back](#)
[Close](#)
[Full Screen / Esc](#)
[Printer-friendly Version](#)
[Interactive Discussion](#)

## Influence of surface albedo heterogeneity on passive remote sensing

C. Fricke et al.

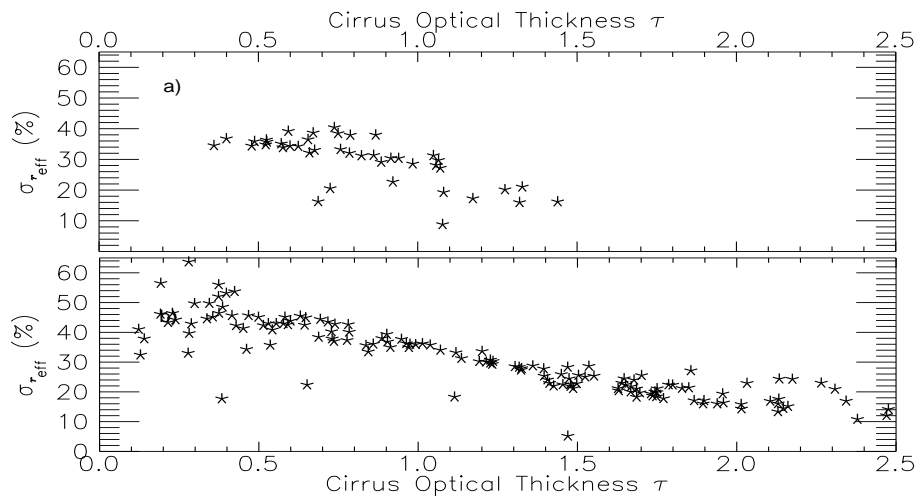


**Fig. 10.** Correlation between standard deviation of  $r_{\text{eff}}$  and  $\tau$  for the 4 November **(a)** and 3 November **(b)** timeseries derived of HALO-SR measurements.

[Title Page](#)[Abstract](#)[Introduction](#)[Conclusions](#)[References](#)[Tables](#)[Figures](#)[⏪](#)[⏩](#)[⏴](#)[⏵](#)[Back](#)[Close](#)[Full Screen / Esc](#)[Printer-friendly Version](#)[Interactive Discussion](#)

## Influence of surface albedo heterogeneity on passive remote sensing

C. Fricke et al.

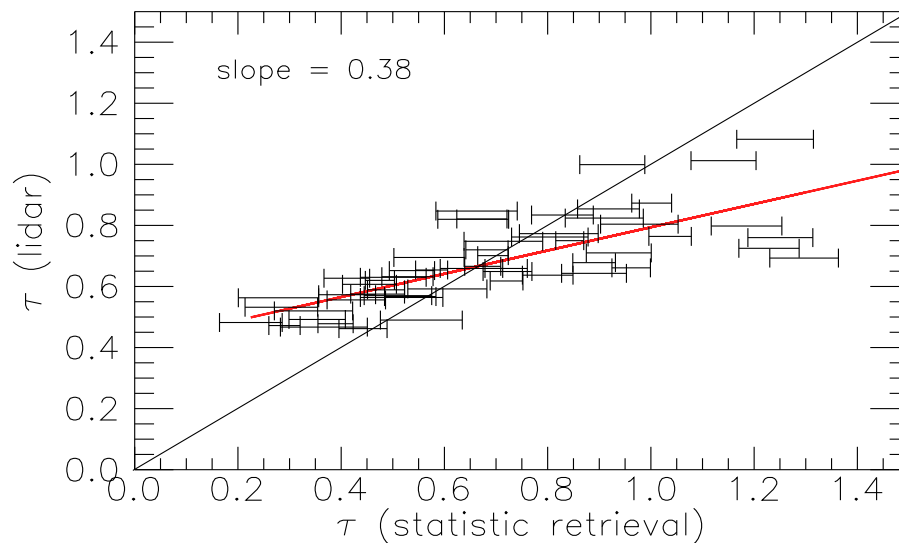


**Fig. 11.** Comparison of  $\tau$  retrieved by the HSRL-lidar and the statistical approach (HALO-SR) for 4 November, 2010. For the simulations a mixture of ice crystal shapes is used.

[Title Page](#)[Abstract](#)[Introduction](#)[Conclusions](#)[References](#)[Tables](#)[Figures](#)[⏪](#)[⏩](#)[⏴](#)[⏵](#)[Back](#)[Close](#)[Full Screen / Esc](#)[Printer-friendly Version](#)[Interactive Discussion](#)

## Influence of surface albedo heterogeneity on passive remote sensing

C. Fricke et al.

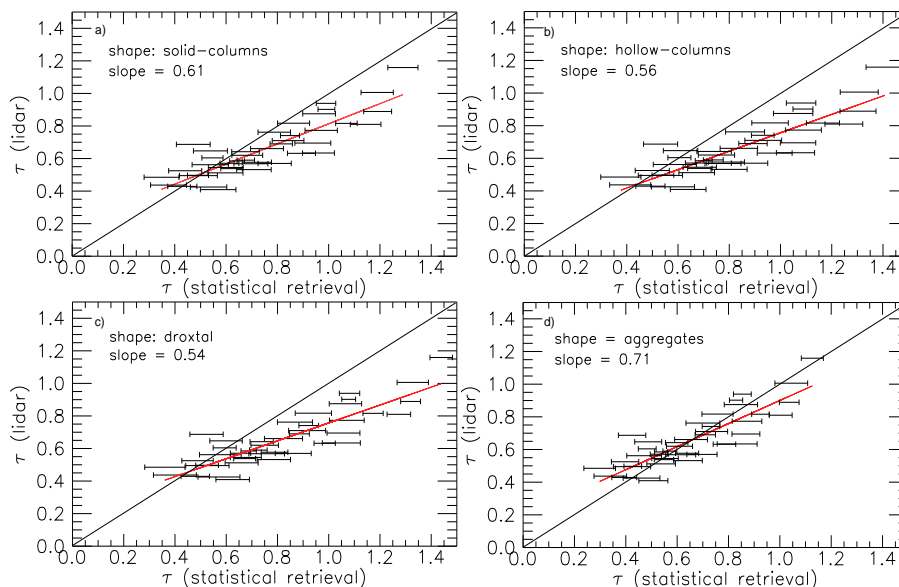


**Fig. 12.** Comparison of  $\tau$  retrieved by the HSRL-lidar and the statistical approach (HALO-SR) for different ice crystal shapes. Droxtals **(a)** show the biggest deviation, hollow **(b)** and solid **(c)** columns slightly improve the slope. The best correlation is achieved for aggregates. The influence increases with increasing  $\tau$ . For values below 0.5 a systematic feature, leading to an underestimation, is beyond the shape influence.

[Title Page](#)
[Abstract](#)
[Introduction](#)
[Conclusions](#)
[References](#)
[Tables](#)
[Figures](#)
[⏪](#)
[⏩](#)
[◀](#)
[▶](#)
[Back](#)
[Close](#)
[Full Screen / Esc](#)
[Printer-friendly Version](#)
[Interactive Discussion](#)

## Influence of surface albedo heterogeneity on passive remote sensing

C. Fricke et al.

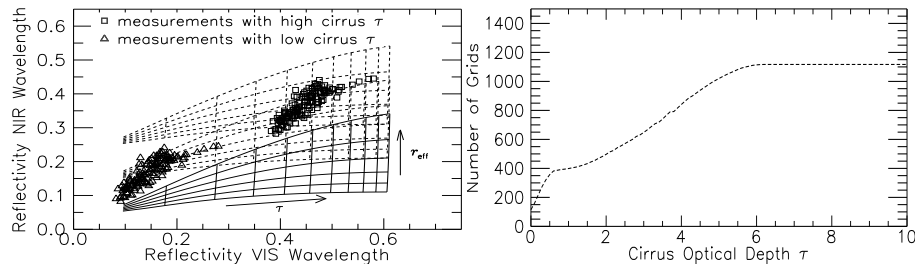


**Fig. 13. (a)** Illustration of systemic retrieval feature leading to an increasing underestimation of results for  $\tau$  below 0.5. Displayed are three radiance grids following the approach of Nakajima and King (1990) for three different assumptions of the surface albedo at 650 nm (0.05, 0.15, 0.25). Measurements for optical thick clouds are shown by squares. Triangles indicate measurements with low optical thickness **(b)** Number of surface albedos leading to a correct solution of the retrieval in dependence of  $\tau$ .

Title Page

Abstract

Introduction

Conclusions

References

Tables

Figures

◀

▶

◀

▶

Back

Close

Full Screen / Esc

Printer-friendly Version

Interactive Discussion

## Influence of surface albedo heterogeneity on passive remote sensing

C. Fricke et al.

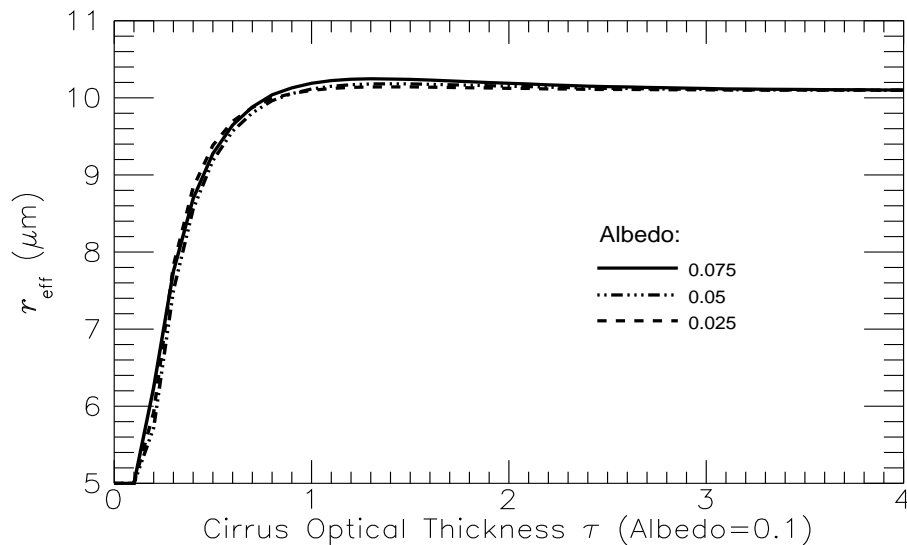


**Fig. 14.** Deviation of  $r_{\text{eff}}$  from a benchmark value of  $10 \mu\text{m}$  and surface albedo of 0.1 for several surface albedo assumptions showing a systematic retrieval feature for  $\tau$  below 0.5.

[Title Page](#)[Abstract](#)[Introduction](#)[Conclusions](#)[References](#)[Tables](#)[Figures](#)[⏪](#)[⏩](#)[⏴](#)[⏵](#)[Back](#)[Close](#)[Full Screen / Esc](#)[Printer-friendly Version](#)[Interactive Discussion](#)

## Influence of surface albedo heterogeneity on passive remote sensing

C. Fricke et al.

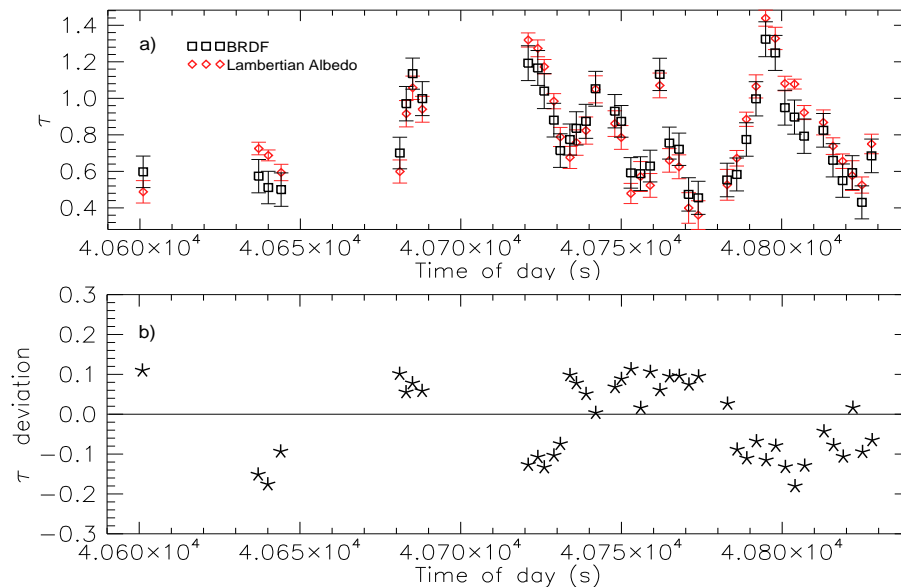


**Fig. 15.** (a) Comparison of mean values and standard deviations between statistic retrieval (HALO-SR) of  $\tau$  using isotropic reflecting surface albedo (red diamonds) and BRDF (black squares) from the 4 November 2010 flight between 11:00 and 11:30 UTC. (b) Corresponding numeric mean value deviation.

## Influence of surface albedo heterogeneity on passive remote sensing

C. Fricke et al.

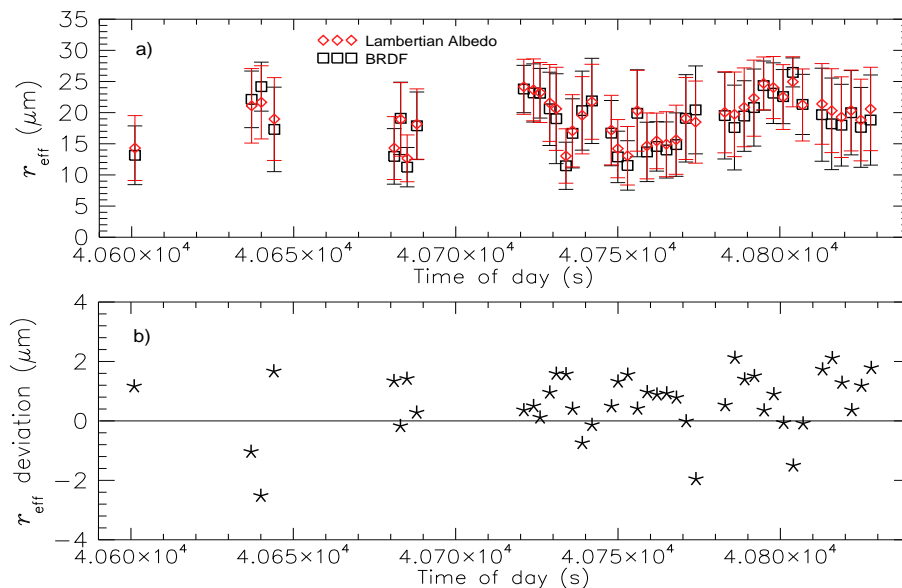


**Fig. 16.** (a) Comparison of mean values and standard deviations between statistic retrieval (HALO-SR) of  $r_{\text{eff}}$  using isotropic reflecting surface albedo (red diamonds) and BRDF (black squares) from the 4 November 2010 flight between 11:00 and 11:30 UTC. (b) Corresponding numeric mean value deviation.

[Title Page](#)[Abstract](#)[Introduction](#)[Conclusions](#)[References](#)[Tables](#)[Figures](#)[⏪](#)[⏩](#)[⏴](#)[⏵](#)[Back](#)[Close](#)[Full Screen / Esc](#)[Printer-friendly Version](#)[Interactive Discussion](#)